CrossMark

Encapsulated phase change material for high temperature thermal energy storage – Heat transfer analysis

Ali F. Elmozughi, Laura Solomon, Alparslan Oztekin *, Sudhakar Neti

Mechanical Engineering and Mechanics, P.C. Rossin College of Engineering and Applied Science, Lehigh University, Bethlehem, PA 18015, USA

ABSTRACT

Thermal analysis of high temperature phase change materials (PCM) is conducted with the consideration of a 20% void and buoyancy-driven convection in a stainless steel capsule. The effects of the thermal expansion and the volume expansion due to phase change on the energy storage and retrieval process are investigated. Sodium nitrate is considered as a potential PCM for concentrated solar power applications. The charging and discharging into and from the capsule wall is simulated for different boundary conditions and is applied with both laminar and turbulent flow conditions. Computational models are conducted by applying an enthalpy-porosity method and volume of fluid method (VOF) to calculate the transport phenomena within the PCM capsule, including an internal air void. Energy storage and retrieval in different sized capsules is simulated. A cylindrical shaped EPCM capsule or tube is considered in simulations using both gas (air) and liquid (Therminol/VP-1) as the heat transfer fluid in a cross flow arrangement. Additionally a spherical shaped EPCM is considered with a constant wall temperature boundary condition to study the three-dimensional heat transfer effects. The presence of the void has profound effects on the thermal response of the EPCM during both energy storage and retrieval process. Melting and solidification per unit mass of the PCM takes longer when the void is present. Additionally, due to material properties and the lack of convective effects, the solidification process is much slower than the melting process.

© 2014 Elsevier Ltd. All rights reserved.

1. Introduction

Nowadays, high temperature applications of solar energy are becoming more attractive and more beneficial for saving energy. Concentrating solar power (CSP) plants use solar radiation as an energy source to heat a thermal fluid that is used in a power generation cycle. CSP plants have implemented several techniques that can concentrate the sunlight upon the thermal receiver from 25 to 3000 time the intensity of natural sunlight [1]. Due to the transient nature of solar radiation, CSP plants have various rangers of peak temperature, and consequently varying thermodynamic efficiencies. Improvements to CSP plants can come from several different aspects, such as tracking the sun, focusing the solar radiation, studying the characteristics of different thermal fluids, or by storing thermal energy during times of high solar radiation. Using thermal storage, a CSP plant can retrieve the stored energy during times of poor solar radiation, such as during a cloudy day or at night, thus increasing the amount of time the plant can produce

electricity. Therefore, energy storage plays a key role to improve the overall efficiency of a CSP power plant and making the use of solar energy more cost-effective.

Most of the TES systems that are currently used at CSP plants today are sensible heat storage systems [1]. Sensible heat storage systems store energy by increasing the temperature of either a solid or liquid material. In order for these systems to store the amount of energy required by CSP plants a large volume of material is needed. In order to reduce the size and cost of these storage systems, one can take advantage of energy stored or released during a phase change. The heat stored and retrieved during the phase change process of a material is called heat of fusion or latent heat. Latent heat energy storage has two main advantages over sensible heat storage: a high storage density and the ability to store energy with only a small temperature variation [2]. In addition, the phase change is an isothermal process, so it takes some time to complete. PCM's have the capability to store and release energy in a wide range of temperature applications. However, there are certain characteristics that a PCM has to exhibit to be suitable for use in a thermocline, for instance: stability, no super-cooling, non-toxicity, and no hazard [2,3].

Nomenclature

G	gravitational acceleration (m/s^2)	γ	liquid fraction
H	convective heat transfer coefficient (W/m^2 K)	ε	a small computational constant
H	total enthalpy (J/kg)	μ	dynamic viscosity (N s/m^2)
H_s	sensible enthalpy (J/kg)	v	kinematic viscosity (m^2/s)
$H_{S_{ref}}$	reference enthalpy (J/kg)	ρ	density (kg/m^3)
K	thermal conductivity (W/m K)	ρ_l	density of liquid phase PCM (kg/m^3)
L	latent heat of fusion (kJ/kg)	ρ_m	density of molten PCM near the melting point (kg/m^3)
$\dot{m}$	mass flow rate (kg/s)		
Nu	Nusselt number	φ	angular coordinate (Rad)
Nu_φ	local Nusselt number		
Pr	Prandtl number		
P	pressure (N/m^2)	*Subscripts*	
R	radius (m)	f	heat transfer fluid
Re	Reynolds number	i	component
S	source term in momentum equations	j	component
T	time (s)	s	capsule surface
T_m	melting temperature (K)	*lower*	below melting point
T_o	initial temperature (K)	*upper*	above melting point
T_{ref}	reference temperature (K)		
U	velocity component (m/s)		
X	x coordinate (m)	*Abbreviations*	
Y	y coordinate (m)	CSP	concentrating solar
		EPCMs	encapsulated phase change materials
		HTF	heat transfer fluid
Greek symbols		PCMs	phase change materials
α	volume fraction	TES	thermal energy storage
β	thermal expansion coefficient (1/K)		

The most common materials studied for use in high temperature applications of PCMs are nitrate salts. However, most salts have a low thermal conductivity which greatly affects the rate of heat transfer and thus the charging and discharging time of the system. By encapsulating the PCM into capsules, compared to a two tank molten salt storage system, the surface area over which heat transfer occurs is increased and thus the charging and discharging time of the system is decreased. However, encapsulation of the PCM has its own challenges such as compatibility between the PCM and capsule materials and the capsule being able to withstand the increase in internal pressure due to the expansion of the PCM during melting. The thermal energy storage research group at Lehigh University has developed a promising technology to store thermal energy in high temperature applications using PCMs [2]. This technique minimizes the volume of storage materials required compared to other sensible heat systems, such as concrete of molten salt storage, and avoids drawbacks that come from the natural behavior of substances like sub-cooling and also has the capability of recyclability and repeated thermal cycles [3]. PCM at high melting temperatures (above 300 °C) are a necessity for operating a CSP plant with thermal energy storage of more than 6 h to produce 100 MWe. The focus of the current work is a heat transfer analysis of two different shapes of EPCMs with an internal air void to accommodate the thermal expansion of the PCM.

Numerically, there are several articles that have discussed heat transfer using phase change materials by applying different techniques such as a fixed grid and an adaptive grid [4]. Moreover, the characteristics of the phase change problem have been investigated by capturing the solid/liquid interface using a method such as front tracking [5]. However, an alternative method is the enthalpy-porosity method which is used in this work. The enthalpy-porosity method was developed by Voller [4,6] and uses an implicit technique for conduction controlled phase change. Additionally, for a comparable time steps this technique is 1.5 to 10 times faster than methods that track the solid/liquid interface.

The enthalpy-porosity method is also referred to by many investigators as a volume tracking method [7]. A fixed-grid solution of the coupled momentum and energy equations as discussed by Brent et al. [6] is undertaken without resorting to variable transformations and by using a two-dimensional dynamic model as well as the influence of laminar natural-convection flow on the melting process of pure gallium in a rectangular cavity. Mackenzie and Robertson [8] solved the nonlinear enthalpy equation using a novel semi-implicit moving mesh discretization at each time step; their results were shown to possess a unique solution. Khodadadi and Zhang [9] studied the effects of buoyancy-driven convection on the constrained melting of PCMs within spherical containers. Their computations were based on an iterative, finite-volume method using primitive-dependent variables and convection accounted for by using Darcy's law and considering a porous medium. They concluded that the effects of Prandtl number on the melting process with consideration of a fixed Rayleigh number as well as the buoyancy-driven convection accelerates the melting process when compared to a melting from pure diffusion models. Ismail [10] studied the solidification of different PCMs in spherical and cylindrical shells of different materials and diameters subject to constant surface temperature. They also investigated how the solidification is affected by the variations of the surface temperature, material and diameter of spherical shells. Tan et al. [11] reported the effect of buoyancy-driven convection by considering the constrained melting of Paraffin wax n-octadecane inside a transparent glass sphere through the use of thermocouples installed inside the sphere. Their results were numerically computed based on an iterative, finite-volume method to solve the enthalpy-porosity equations. Pinelli and Piva [12] implemented the enthalpy-porosity methodology into FLUENT to study thermal energy storage into PCM (n-octadecane, paraffin wax) in a cylindrical capsule using uniform heat transfer coefficient along the outer surface of the capsule. Assis et al. [13] employed FLUENT to produce a parametric investigation of the melting of the low

temperature PCM (RT27) in spherical shells. Their simulations incorporated such phenomena as convection in the liquid phase, volumetric expansion due to melting, considering 15% void, using a specific constant temperature at the boundary and they compared their computational models with experimental results. Their model attempts to solve the complete transient conservation equations simultaneously for solid PCM, liquid PCM, and air, while allowing for PCM expansion, convection in the fluid media (melted PCM and air), and solid phase motion in the liquid. Zhao et al. [5] reported on the heat transfer analysis of EPCMs for thermal energy storage at high temperature using both front tracking and enthalpy-porosity methods. The effects of a void on the EPCM heat storage are not included in their work.

The main goal of this paper is to conduct a thermal analysis for a high temperature EPCM capsule by considering a 20% air void. In order to examine the effects of thermal expansion and the volume expansion due to melting of the PCM on the heat transfer an internal void space is necessary. Without a void, the rise in internal pressure would result in capsule failure [14]. The void fraction within the capsule is determined based on the thermal expansion coefficient (β) of the chosen PCM under investigation. In this case PCM is the sodium nitrate ($NaNO_3$) and $\beta = 4.0 \times 10^{-4}$ 1/K. For the temperature range used in this study the total volume change is about 10%. However, in actual applications the expansion from room temperature needs to be considered. From room temperature until the maximum temperature of 773 K, the total expansion is around 18%. A 20% void is used in the EPCM capsule to avoid high pressures in the capsule. The level of void in the EPCM capsule varies with time during melting and solidification process. Two-dimensional transient heat transfer simulations are applied to different sizes of capsules using two different heat transfer fluids (HTF), liquid (Terminal/VP-1) and gas (air). Additionally, comparison of the charging and discharging times with and without a void is conducted for the two-dimensional case to demonstrate the effect of the internal void on the heat transfer within the EPCM capsule. Furthermore, a separate case of the melting and solidification in a three dimensional capsule with constant wall temperature is considered. The results illustrated would assist in the designing of a latent heat thermocline storage system for a CSP plant as well as other applications.

2. Mathematical modeling and numerical solutions

The heat transfer analysis of an EPCM capsule with an internal air void is being studied by modeling the phase changes within the capsule for various geometries and boundary conditions. An example of the computational domain being investigated is presented in Fig. 1. This figure depicts a cylindrical capsule placed in a cross flow with the heat transfer fluid. Both a gaseous and a liquid fluid were investigated as heat transfer fluids. Additionally, the phase change within a sphere with a constant surface temperature was examined. A 20% internal air void located at the top of the capsule was considered in every case.

The PCM is assumed to be a pure substance (no moisture or impurities) so any sub-cooling effects are neglected. The capsule and HTF are considered to be incompressible and the Boussinesq approximation is adopted for the buoyancy-driven convection in the molten PCM with gravity effects. The volume of fluid (VOF) method is applied to treat the multiphase media which consists of air, being treated as an ideal gas, and the molten salt expansion (liquid region).

A numerical solution is obtained using the enthalpy-porosity method and VOF approach simultaneously. The computational domain in the PCM will be divided into three regions; a solid, a liquid, and a mushy zone (porous medium). As the temperature
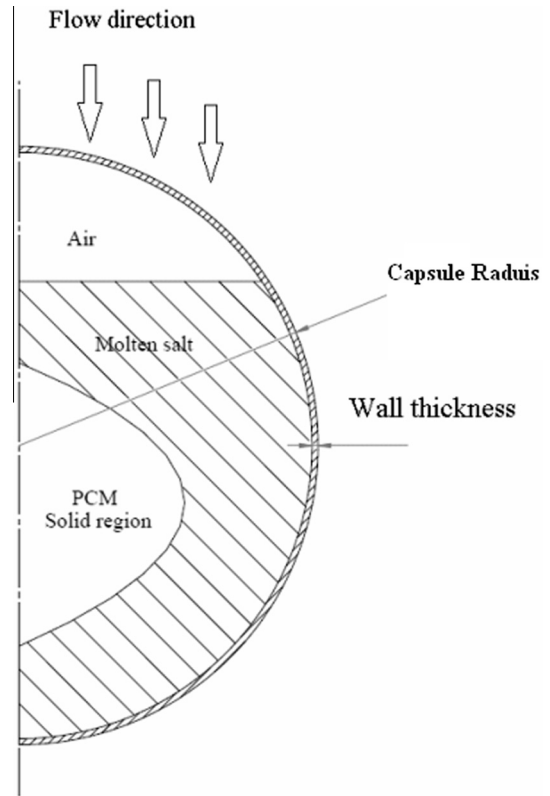
Fig. 1. Computational MODEL of EPCM with void.

distribution is determined, the liquid fraction, γ, can be calculated. Thus the solid, liquid, and mushy zones can be identified. A value of $\gamma = 0$ and 1 denotes the solid and the liquid regions, respectively, while $0 < \gamma < 1$ denotes the mushy zone.

The system (PCM molten salt–air) is described as a multiphase problem with a moving internal interface without interpenetration. The fraction of volume is applied in one set of equations [15] based on α_q. Either $\alpha_q = 0$ for the empty cell from the qth fluid, $\alpha_q = 1$ for the full cell of the qth fluid, or $0 < \alpha_q < 1$ which means the cell contains the interface between the qth fluid and another fluid. Therefore, the following sets of equations represent the system for simulating $NaNO_3$ [15]:

$$\frac{\partial \alpha_q}{\partial t} + u_i \frac{\partial \alpha_q}{\partial x_i} = 0 \tag{1}$$

$$\frac{\partial}{\partial t}(\rho u_i) + \frac{\partial}{\partial x_i}(\rho u_j u_i) = \mu \left(\frac{\partial^2 u_i}{\partial x_j \partial x_j} \right) - \frac{\partial P}{\partial x_i} + \rho g_i + S_i \tag{2}$$

$$\frac{\partial}{\partial t}(\rho H) + \frac{\partial}{\partial x_i}(\rho u_i H) = \frac{\partial}{\partial x_i} \left(k \frac{\partial T}{\partial x_i} \right) \tag{3}$$

$$H = H_{S_{ref}} + \int_{T_{ref}}^{T} c \, dT + \gamma L \tag{4}$$

where H is the total enthalpy; $H_{S_{ref}}$ is the reference enthalpy; L is the latent heat of fusion; T_{ref} is the reference temperature and T is the temperature. γ is determined by the following set of equations:

$$\begin{bmatrix} \gamma = 0 & if \ T < T_{lower} \\ \gamma = 1 & if \ T > T_{upper} \\ \gamma = \frac{T - T_{lower}}{T_{upper} - T_{lower}} & if \ T_{lower} < T < T_{upper} \end{bmatrix} \tag{5}$$

where T_{lower} and T_{upper} are temperatures slightly below and above the melting temperatures, respectively. The values of these

temperatures determine the size of the mushy region and it is selected by the algorithm based on the heating/cooling rate and the physical properties of the PCM.

With the Boussinesq approximation the equations governing the buoyancy-driven convection in the molten PCM are written for an incompressible fluid. Where u_i is the velocity vector; v is the kinematic viscosity of the molten PCM; p is the pressure; g_i is the gravitational acceleration vector; ρ_m is the reference density of PCM determined at the melting temperature.

$\rho_l = \rho_m - \rho_m \beta (T - T_m)$ [6,7] is the temperature dependent density of the molten PCM and β is the thermal expansion coefficient of the molten PCM ($\beta = 4.0 \times 10^{-4}$ 1/K for liquid NaNO$_3$). The momentum source vector in Eq. (2) is modeled as $S_i = -A(\gamma)u_i$ [6,7] with the porosity function $A(\gamma) = C(1 - \gamma)^2/(\gamma^3 + \varepsilon)$ [6,7] where C is a constant value denoting the morphology of the melting front and ε is a small computational constant [15]. The values of C and ε are chosen 10^4 and 0.0001, respectively, in the present study. The porosity function reduces the velocity to zero at a solid region. $A(\gamma)$ makes the momentum equation (Kozeny–Carman equation) for flow in porous media [15].

The physical properties of the chosen PCM and capsule, NaNO$_3$ and stainless steel, are listed in Table 1. For the 2-D simulations, two different types of HTF are used: air and Therminol/VP-1. The thermodynamic properties of the HTFs are displayed in Table 2.

3. Validation of the model

In order to validate the present numerical technique, numerical simulations are conducted for RT27_Rubitherm GmbH as the PCM and compared against the predicted and measured results reported by Assis et al. [21]. A spherical shaped plastic EPCM of 40 mm in diameter is used. As the PCM does not have a constant melting temperature, therefore a melting interval is used, with the solidus and liquids temperatures set at 28 °C and 30 °C, respectively. In the simulation, the initial temperature of the computational model is 32 °C; however, the boundary condition is a specific temperature of 15 °C.

Fig. 2 depicts the contours of the liquid/solid interface at various times. The interface contours are predicated by using the present methods of enthalpy-porosity and volume of fluid simultaneously. These results are verified with the solidification process for paraffin by Assis et al. [21] to validate the numerical technique at different times such as 600 s and 1500 s. It was concluded that the results qualitatively have a good agreement with results reported in [21]. Additionally, after 600 s the PCM is 58% solidified and after 1500 s it is 90% solidified. According to the results presented by Assis after their PCM was 95% solidified after 1500 s [21]. The agreement between the percent PCM solidification further verifies the numerical technique in use. Additionally, Assis et al. confirmed this numerical technique in pervious paper as well [13].

4. Results and discussion

The heat transfer analysis is presented for NaNO$_3$ encapsulated by a stainless steel shell. A 2-dimensional simulation of a cylindrical capsule is presented for two capsule diameters, 25.4 mm and 76.2 mm, with both having a shell thickness of 1.5875 mm. A

Table 2
Physical properties of heat transfer fluid: air [19] and Therminol/VP-1 [20].

	Air (1 atm, 773 K)	Therminol/VP-1 (698 K)
Density (kg/m^3)	0.4	654
k (W/m K)	0.06	0.07
c (J/kg K)	1093	2760
Viscosity (N s/m^2)	3.6×10^{-5}	1.3×10^{-4}
Prandtl number, Pr	0.7	5.3
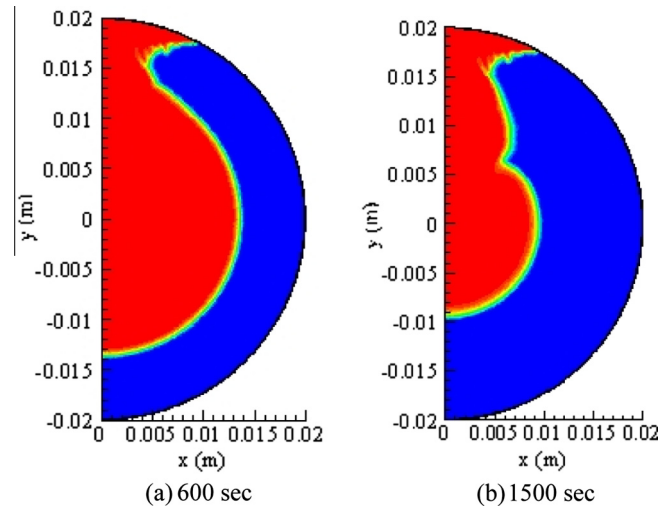
Fig. 2. The location of the solid/liquid interfaces at: (a) 600 s and (b) 1500 s.

3-dimensional analysis is conducted for a 22 mm sphere with a shell thickness of 1 mm. In order to complete the simulations the properties such as specific heat, thermal conductivity, melting temperature, and density of both materials are needed, and listed in Table 1. Additionally, the melting temperature of NaNO$_3$ is 308 °C.

A cross flow arrangement of the HTF around the capsule is considered. The temperature of the HTF is 500 °C for a charging process while it is 250 °C for a discharging process. The initial temperature of the capsule is at 250 °C for the charging process and 500 °C for a discharging process. The HTF flows from the top to the bottom of the cylinder during both the charging and discharging process. Based on the local Nusselt number, the heat transfer coefficients around the capsule is determined [22,23]. The Reynolds number of the flow is also calculated by using a superficial velocity in the thermocline system for the mass flow rate of the heat transfer fluid (0.1–0.5 kg/s) and the diameter of the capsule. Fig. 3 displays the distribution of the heat transfer coefficients of air and VP-1 around the 76.2 mm diameter capsule.

The enthalpy-porosity and VOF methods are applied to predict the charging and discharging times of the stainless steel-NaNO$_3$ EPCM capsules with an internal air void. Buoyancy-driven convection, gravitational effects, and variable density NaNO$_3$ with thermal expansion during melting are considered. Therefore, the energy stored and released to and from each cell is calculated by solving Eqs. (1)–(5) simultaneously using an iterative method. Iteration at each time step continues until the residuals reach values

Table 1
Physical properties of the NaNO$_3$ and the stainless steel.

	Density (kg/m^3)	Thermal conductivity (W/m K)	Specific heat (J/kg K)	Viscosity (kg/m s)	Latent heat (kJ/kg)
Solid NaNO$_3$	2260 [16]	0.5 [17]	1588 [18]	–	162.5 [18]
Liquid NaNO$_3$	1900 [17]	0.5 [17]	1650 [18]	0.00285 [17]	
Stainless steel	7900 [19]	14.9 [19]	477 [18]	–	–

Air as HTF for Re=1,230   VP-1 as HTF for Re=29,752
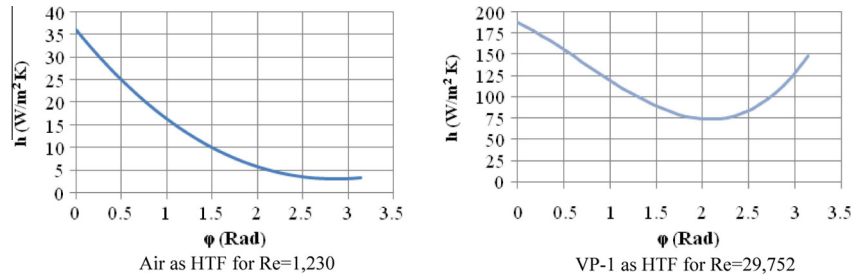
Fig. 3. The distribution of the heat transfer coefficient around the capsule for 76.2 mm.

(a) 2290 nodes   (b) 4276 nodes   (c) 8736 nodes
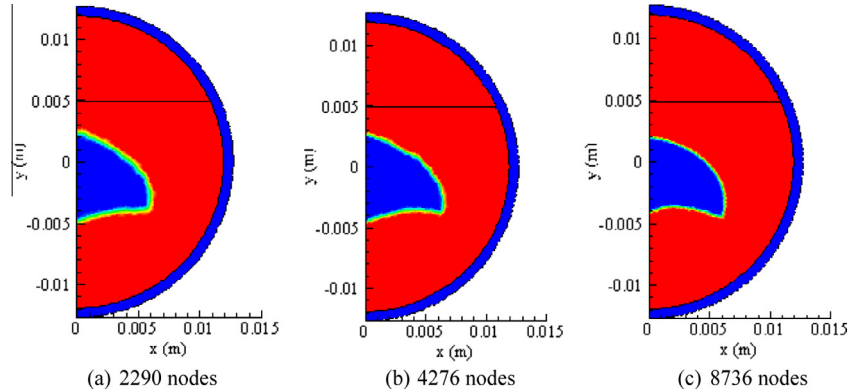
Fig. 4. The location of the liquid/solid interface with 20% void.

below 10^{-6} for the energy equation and 10^{-3} for both the continuity and the momentum equations at each node. A triangular meshing for the capsules is used.

The spatial and the temporal convergence of the numerical method are tested. Fig. 4 depicts the spatial convergence of the solid/liquid interface at the same time instant for a 25.4 mm capsule computational model with a 773 K uniform temperature boundary condition and a 523 K initial temperature for a varying number of nodes: 2290, 4276 (chosen), and 8736. The co-centering blue region is solid zone; molten salt is referred to by the red color, and the blue boundary refers to the stainless steel shell. Furthermore, the total melting time for all three cases is the same; 49.5 s with time step 0.02 s.

Simulation results with the 4276 node using time steps of 0.01, 0.02, and 0.03 show insignificant differences, implying that time step of 0.01 is sufficient to satisfy the temporal convergence for the system. The number of nodes in the 76.2 mm two-dimensional cylindrical capsule and 22 mm three-dimensional spherical capsule is 11,000 and 15,376 respectively.

4.1. Cylindrical EPCM

First, the results of two dimensional heat transfer analysis are presented. Fig. 5 shows the instantaneous contours of the velocity magnitude and temperature distributions for a 25.4 mm cylindrical capsule with two different heat transfer fluids, air and VP-1. The right half of the EPCM capsule represents the temperature contours and left side represents the velocity magnitude. Although the rate of heat transfer is smaller at the top of the EPCM capsule, the temperature gradient is larger compared to the rest the PCM. Here, the poor thermal conductivity of the air at the top (void region) reduces the rate of heat transfer as shown in Fig. 5(a) and (b).

The temperature of the molten $NaNO_3$ salt increases rapidly as the melting process progresses, while the temperature of solid $NaNO_3$ remains nearly constant. The velocity magnitudes are very low in both the air and molten PCM; however, it still affects the melting process. The rate of heat transfer has a significant influence on the temperature and velocity contours during the melting process. The higher rate of heat transfer with VP-1 as the HTF enhances buoyancy-driven convection which creates small vortices at the bottom of the solid PCM and accelerates the temperature reaching the melting point in a shorter time as compared to with air as the HTF. These results are illustrated in Fig. 5 (a)–(d).

Fig. 6(a)–(g) show the location of the liquid/solid interfaces at different instances in time. The liquid/solid interface is shown on the left side for a 25.4 mm cylindrical EPCM capsule while density variations are shown on the right side. The location of the liquid/solid interface and the interface separating air from PCM are identified by the density of each phase. During the charging process, the volume expansion due to phase change and the thermal expansion of the salt drive the molten salt region to occupy 20% of the initial void space and the air become compressed at the top of the capsule.

As shown in Fig. 6(b) and (f), the solid PCM region is shaped with regard to the rate of the surface heat transfer. Additionally, Fig. 6(c) shows that buoyancy-driven convection with air as the HTF is not strong enough to create clear vortices at the bottom of the capsule and the solid PCM is sinking close to the bottom wall of the capsule. In contrast, with VP-1 as the HTF the solid PCM is bounced up as shown in Fig. 6(g) due to the increased heat transfer enhancing the vortices to increase the melting process at the bottom of the PCM.

Temperature distributions and velocity magnitudes in the 76.2 mm $NaNO_3$ EPCM capsule are similar to that of a 25.4 mm capsule. The intensity of eddies formed near the bottom of the capsule are greater and the characteristics of the flow in the molten salt is different in the larger size capsule. Small vortices at the bottom of the solid PCM are formed at the early stage and they become larger as melting progresses and assist to increase re-circulation of the molten salt to accelerate propagation of the solid/liquid front (not presented).

(a) air as HTF (Re = 1230) at 200 s   (b) air as HTF (Re = 1230) at 3600 s

(c) VP-1 as HTF (Re=29,752) at 25 s   (d) VP-1 as HTF (Re=29,752) at 180 s
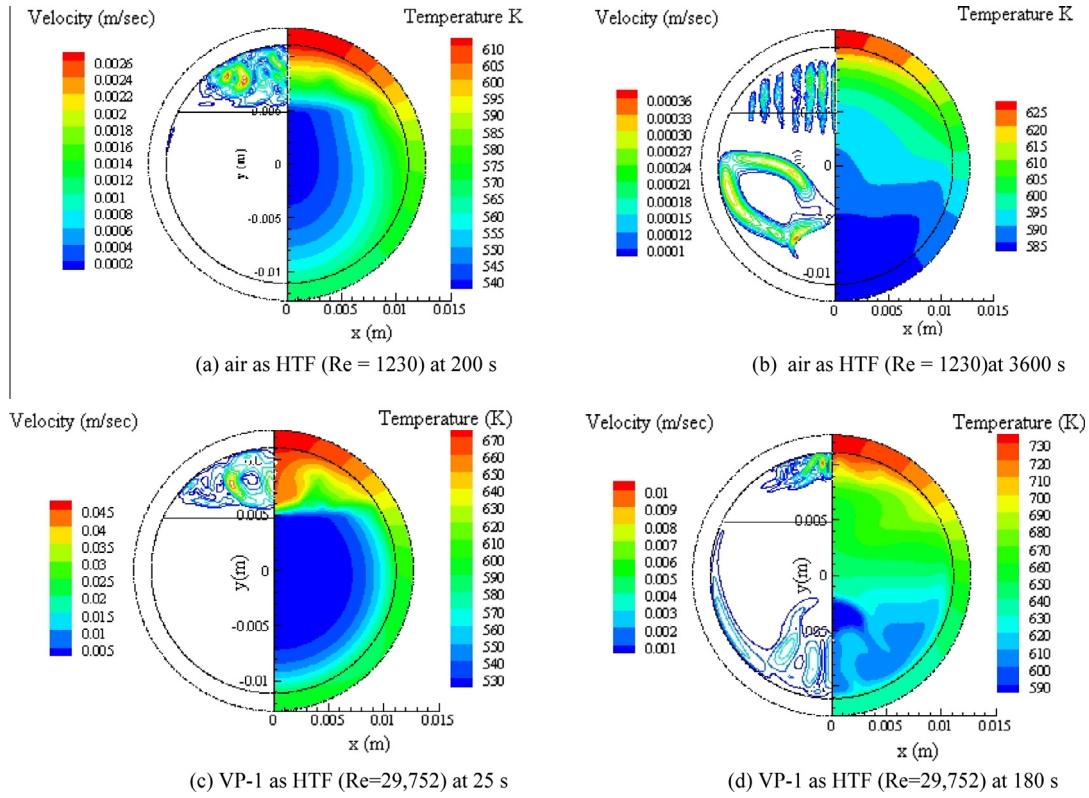
Fig. 5. The isotherms and the contours of the velocity magnitude in NaNO$_3$ EPCM with 20% void.

air as HTF

(a) t =200s (19% void)   (b) t = 1200s (10% void)   (c) t = 3600s (7% void)

VP-1 as HTF

(e) t = 25s (19% void)   (f) t = 95s (10% void)   (g) t = 182s (5% void)
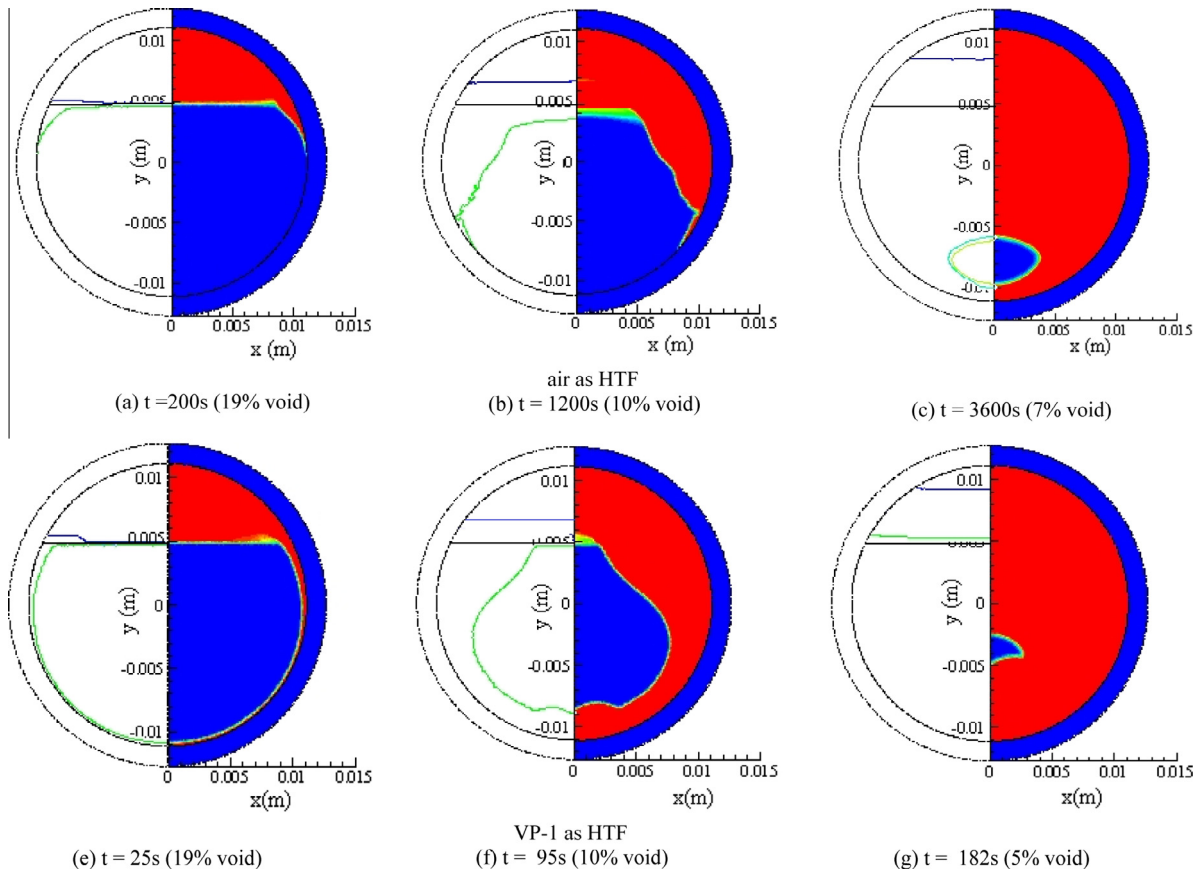
Fig. 6. Density distribution and the location of the liquid/solid interfaces in NaNO$_3$ EPCM with 20% initial void.
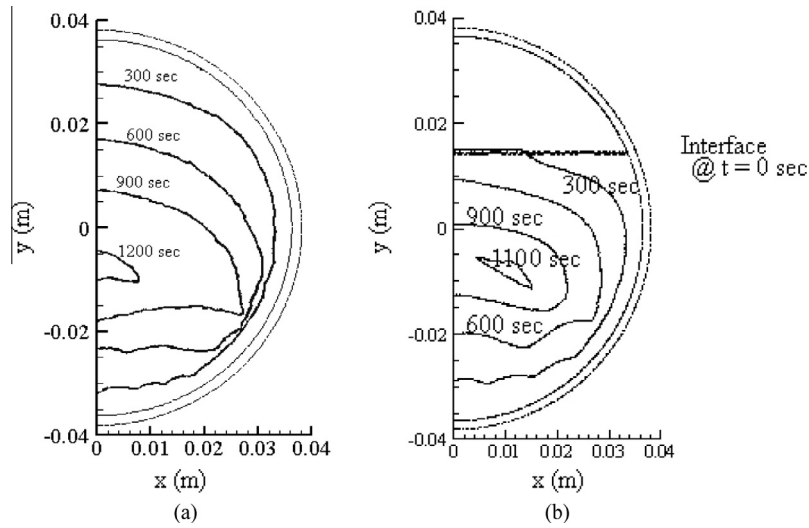
Fig. 7. The location of the propagating liquid/solid interface at various times for: (a) without void, and (b) with 20% void (air).

The evolution of the liquid/solid interfaces is also similar to that of the smaller capsule for both air and VP-1 as HTF. The total melting time of the 76.2 mm diameter EPCM capsule with VP-1 as the HTF is 1260 s, which is 6.8 times longer than that of the 25.4 mm capsule.

Fig. 7(a) and (b) shows a comparison of the location of the propagating liquid/solid interface between an EPCM capsule with and without a void at several times predicted by the enthalpy-porosity method with VOF for a 76.2 mm diameter cylindrical NaNO₃ capsule during a charging process using liquid VP-1 as the HTF. The dynamics of the interfaces in both the capsule with and without the void are different. In Fig. 7(a), the re-circulating vortices reshape the liquid/solid interface from concentric rings to a mushroom shape. The vortices become larger at the bottom of PCM after 600 s. However, in the Fig. 7(b) at the top of the capsule the liquid/solid interface slowly moves because air plays the main role in reducing the melting progress along the air/PCM interface. The motion of vortices at the bottom of the capsule causes the solid PCM to separate into two parts.

Fig. 8 shows contours of temperature and streamlines for a capsule with and without a void. Here, the temperature contours in the capsule without a void at 600 s shows a nearly concentric ring pattern with a slight distortion at the bottom due to the accelerated melting aided by the eddies. These effects are amplified in the capsule with the void as shown in Fig. 8(a). Streamlines and temperature contours become slightly different in both cases. Fig. 8(a) shows that in a PCM capsule with a void, buoyancy-driven convection drives to create much bigger vortices than in a capsule without void. In the capsule with a void, the melting progress is much faster at the center of the capsule.

Thermocline consisting of several cylindrical rods is built and the thermal measurements are conducted in our lab. Numerical simulations of the thermocline are conducted and the predicted results are compared against the measured results for the thermal behavior of the energy storage module. The results will be presented in a full paper. System model does not include important thermal features such as those considered in the present study (*the presence of void and the buoyancy-driven convection in an individual EPCM*) due to the limitations of computational resources.

4.2. Spherical EPCM

To study the 3-dimensional effects on the melting and solidification process, the case of a 22 mm sphere with a void and a constant surface temperature was examined. For the melting case a constant wall temperature of 750 K and an initial temperature of 523 K were used. For solidification the temperatures are reversed. Due to symmetry about the Y axis, the heat transfer in the XY and

(a) With void at 600 sec   (b) Without void at 600 sec
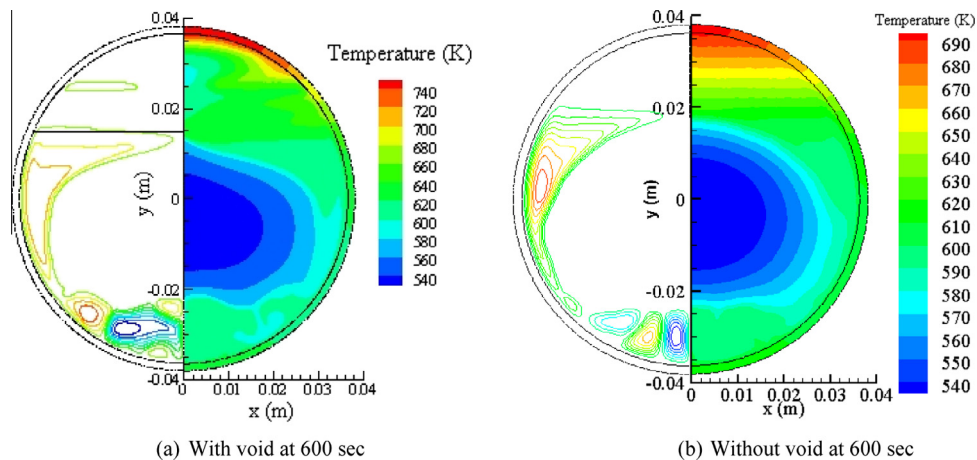
Fig. 8. The isotherms and the streamlines in NaNO₃ EPCM.

(a) The isotherms on XY (upper) & ZX (lower) planes

(b) The contours of the velocity magnitude on XY (upper) & ZX (lower) planes

(c) The interfaces on XY (upper) & ZX (lower) planes

(d) Liquid Faction on XY (upper) & ZX (lower) Planes
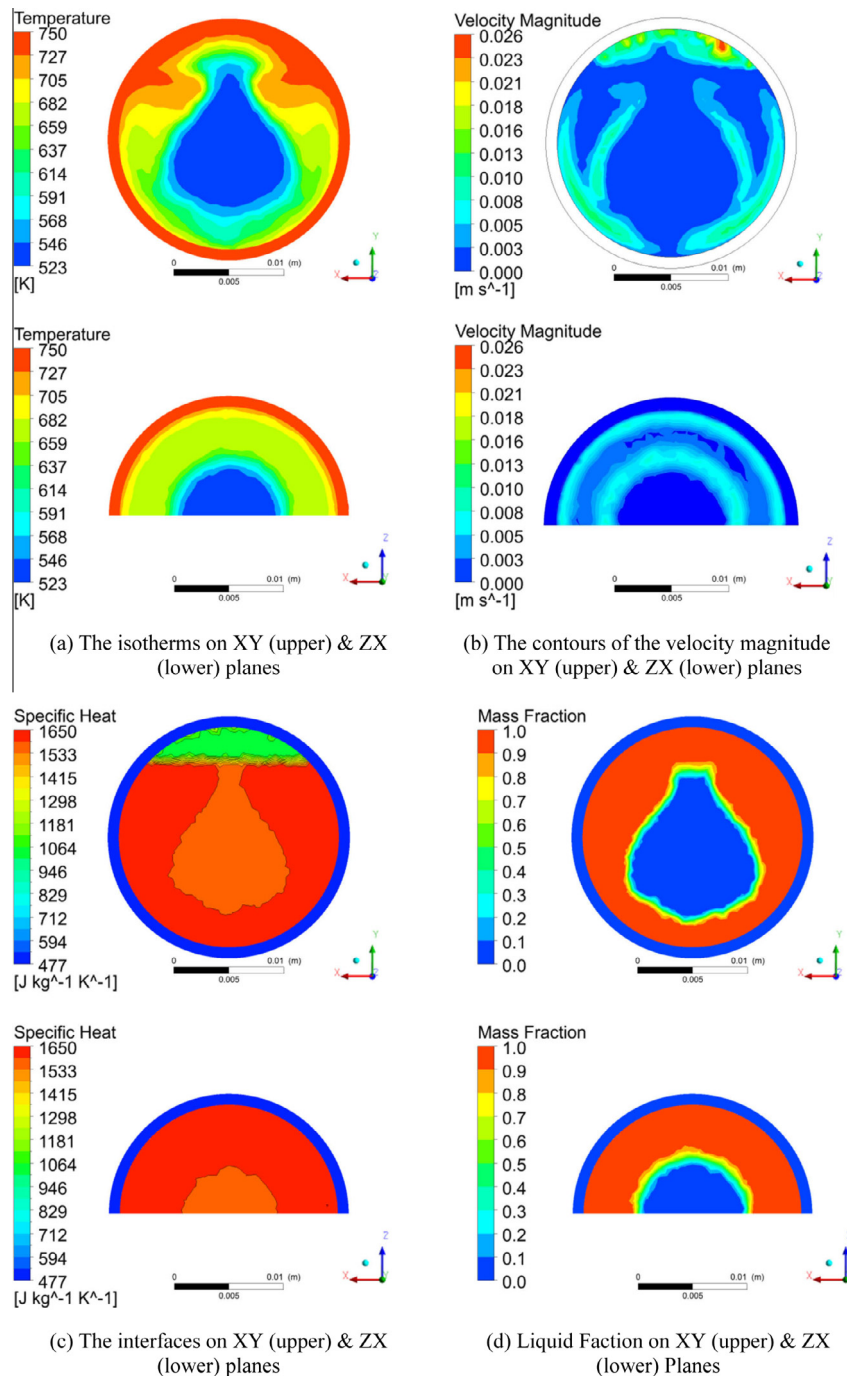
Fig. 9. The isotherms, the velocity magnitude, the interfaces and the liquid fraction at 15 s into melting. (For interpretation of the references to color in this figure legend, the reader is referred to the web version of this article.)

YZ planes is identical. Therefore, only the results for the *XY* plane are shown. Fig. 9(a)–(d) shows the temperature, velocity magnitude, specific heat, and liquid fraction contours 15 s into the melting process. Since the specific heat is constant for each material and phase, the contour plot shows the interfaces between the solid NaNO$_3$, liquid NaNO$_3$, and the air void. In Fig. 9(c) the blue represents that stainless steel shell, green represents the air void, orange the solid PCM, and red shows the liquid PCM. The melting begins at the corner of the PCM-void interface on the *XY* plane. Since there is no void in the *ZX* plane, the temperature contour forms concentric rings about the center of the sphere.

As the melting process progresses, natural convection in the molten salt enhances the heat transfer rate. These re-circulating vortices that begin at the corner of the PCM-void interface causes the PCM to melt faster than along the bottom of the edge of the sphere creating a tear drop shaped solid region in the *XY* plane, as shown Fig. 9(a)–(d). In Fig. 9(d), the solid phase is depicted in blue with the liquid phase shown in red. While the solid region has a tear drop shape in the *XY* plane, it has a circular shape in the *ZX* plane due to the lack of an air void acting as an insulator.

At later stages of the melting process, a small vortex forms at the bottom of the sphere that keeps the remaining solid PCM from

(a) The isotherms

(b) The contours of the velocity magnitude

(c) The interfaces

(d) The liquid faction
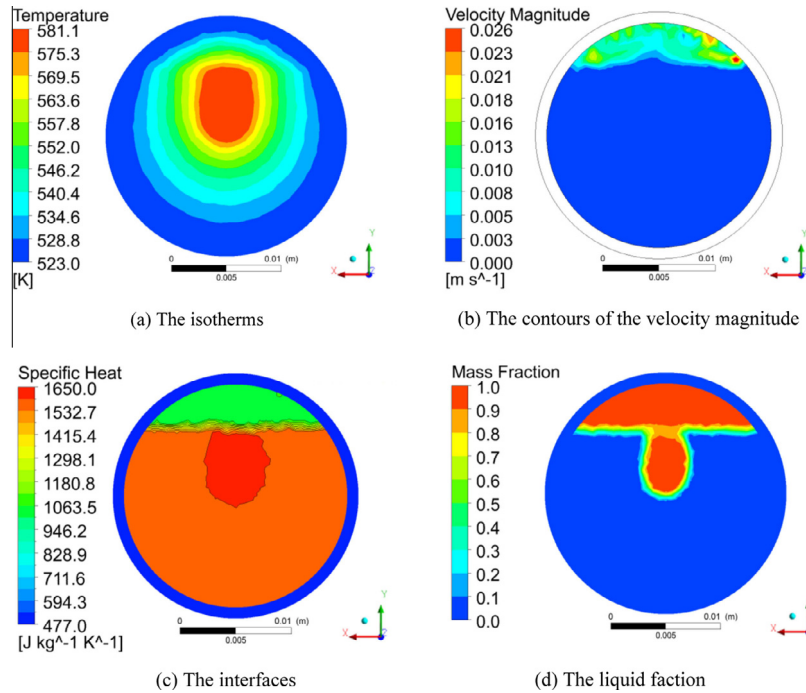
Fig. 10. The isotherms, the velocity magnitude, the interfaces and the liquid fraction on the *XY* plane at 240 s into solidification.

(a) t = 5s (12.9% void)

(b) t = 15s (7.9% void)

(c) t = 25s (6.1% void)

(d) t = 5s (6.7% void)

(e) t = 60s (9.9% void)

(f) t = 240s (11.4% void)
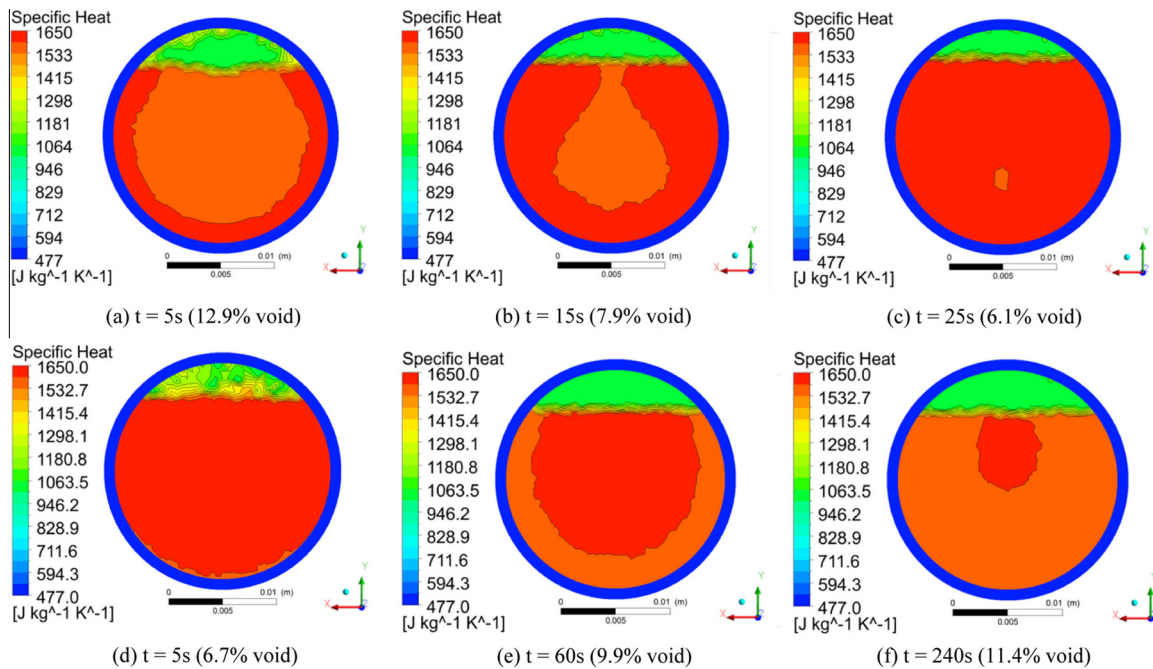
Fig. 11. The interfaces during (a)–(c) melting and (d)–(f) solidification at various times.

sinking, while also increasing the heat transfer rate. The greater rate of heat transfer in the *ZX* plane results a slightly faster melting time than in the *XY* plane. The total melting time for the 22 mm diameter sphere was 30 s. The volume of the PCM increased 10% resulting in the air void being compressed by 50%.

After the melting of the sphere was completed, it was heated to 750 K throughout before beginning the solidification process. When the boundary temperature is changed to 523 K the temperature of the PCM drops rapidly. Solidification of the PCM begins at the bottom of the shell and gradually moves upward. The initial temperature changes cause small vortices to form at the walls of

the shell as the rapidly cooling PCM becomes denser and sinks. One minute into the solidification process the temperature of the solid PCM is nominally 581 K, the melting point of NaNO$_3$. After this initial cooling period the solidification of the remaining liquid PCM begins to slow down due to the poor thermal conductivity of the salt and lack of convective effects. As solidification progresses, the PCM solidifies radially inward. In the *ZX* plane the heat transfer is uniform around the entire sphere yielding a circular solidification pattern. However, in the *XY* plane the air void at the top acts as an insulator and reduces the heat transfer rate resulting in a horseshoe shaped solid region.

As the solidification process continues the growing solid region decreases the heat transfer rate which increases the total solidification time. Fig. 10(a) depicts the temperature contour 240 s into the solidification process. The air void at the top greatly reduces the amount of heat transferred from the top of the shell to the PCM. This results in the PCM mostly solidifying from the bottom up, as seen in Fig 10. The total solidification time for the 22 mm sphere is 300 s, 10 times longer than the melting time. Fig. 11 depicts the evolution of the interfaces between the air void, solid PCM, and liquid PCM throughout the entire melting and solidification processes. Spatial and temporal characteristics of the interface are influenced by the presence of void and the buoyancy-driven convection in the molten PCM. Due to the thermal expansion of the PCM during the melting process, the volume percentage of the air void decreases from 12.9% at 5 s to 6.1% at 25 s. Similarly, during solidification the PCM contracts and the void expand from 6.7% after 5 s to 11.4% after 240 s.

5. Conclusion

Using the enthalpy-porosity and volume of fluid methods in ANSYS FLUENT, a heat transfer analysis of the melting and solidification of a $NaNO_3$-stainless steel EPCM capsules was carried out. Two-dimensional simulations of a 25.4 and 76.2 mm cylindrical EPCM capsules with an internal air void were conducted using two different heat transfer fluids, air and VP-1. The shape of the solid/liquid interface is determined by the rate of heat transfer. The higher rate of heat transfer achieved with VP-1 as the HTF increases natural convection within the molten salt, thus reducing the total melting time. Additionally, the presence of the air void at the top of the capsule reduces the heat transfer at the top of the capsule. The void also affects the shape of the solid/liquid interface, changing it from a circular shape to a mushroom shape.

The 3-dimensional heat transfer effects were examined by simulating the melting and solidification of a 22 mm sphere with a constant wall temperature. As with the 2-dimensional case, the shape of the solid/liquid interface is influenced by the rate of heat transfer. The presence of the void at the top of the sphere results in a difference in the heat transfer rates on the *XY* and *ZX* planes. The thermal expansion of the PCM during phase change reduced the initial void volume by 50%, resulting in the air being compressed at the top of the sphere. During the solidification process, the temperature difference between the melting point of the PCM and the capsule wall is 100 K smaller than during the melting process, resulting is a lower rate of heat transfer. In addition to this slower heat transfer rate, a lack of natural convection in the liquid PCM and the low thermal conductivity of the PCM results in a solidification time that is 10 times longer than the melting time.

Conflict of interest

None declared.

References

[1] I. Dincer, M.A. Rosen, Thermal Energy Storage: Systems and Applications, John Wiley & Sons, 2011.
[2] W. Zhao, Y. Zheng, J. C. Sabol, A. Oztekin, S. Neti, K. Tuzla et al., Heat transfer analysis for thermal energy storage using $NANO_3$ as encapsulated phase change material, in: ASME 2012 Heat Transfer Summer Conference collocated with the ASME 2012 Fluids Engineering Division Summer Meeting and the ASME 2012 10th International Conference on Nanochannels, Microchannels and Minichannels, 2012, pp. 241–248.
[3] A. Sharma, V.V. Tyagi, C.R. Chen, D. Buddhi, Review on thermal energy storage with phase change materials and applications, Renewable Sustainable Energy Rev. 13 (2009) 318–345.
[4] V.R. Voller, C. Prakash, A fixed grid numerical modeling methodology for convection–diffusion mushy region phase-change problems, Int. J. Heat Mass Transfer 30 (1987) 1709–1718.
[5] W. Zhao, A.F. Elmozughi, A. Oztekin, S. Neti, Heat transfer analysis of encapsulated phase change material for thermal energy storage, Int. J. Heat Mass Transfer 63 (2013) 323–335.
[6] A.D. Brent, V.R. Voller, K.J. Reid, Enthalpy-porosity technique for modeling convection-diffusion phase change: application to the melting of a pure metal, Numer. Heat Transfer 13 (1988) 297–318 (2014/04/06).
[7] V. Alexiades, A.D. Solomon, Mathematical Modeling of Melting and Freezing Processes, Hemisphere Publishing Corporation, Washington, DC, 1993.
[8] J.A. Mackenzie, M.L. Robertson, The numerical solution of one-dimensional phase change problems using an adaptive moving mesh method, J. Comput. Phys. 161 (2000) 537–557.
[9] J.M. Khodadadi, Y. Zhang, Effects of buoyancy-driven convection on melting within spherical containers, Int. J. Heat Mass Transfer 44 (2001) 1605–1618.
[10] K.A.R. Ismail, Heat Transfer in Phase Change in Simple and Complex Geometries. Thermal Energy Storage Systems and Applications, Wiley, Chichester, 2002.
[11] F.L. Tan, S.F. Hosseinizadeh, J.M. Khodadadi, L. Fan, Experimental and computational study of constrained melting of phase change materials (PCM) inside a spherical capsule, Int. J. Heat Mass Transfer 52 (2009) 3464–3472.
[12] M. Pinelli, S. Piva, Solid/liquid phase change in presence of natural convection: a thermal energy storage case study, J. Energy Res. Technol. 125 (2003) 190–198.
[13] E. Assis, L. Katsman, G. Ziskind, R. Letan, Numerical and experimental study of melting in a spherical shell, Int. J. Heat Mass Transfer 50 (2007) 1790–1804.
[14] J.J. Blaney, S. Neti, W.Z. Misiolek, A. Oztekin, Containment capsule stresses for encapsulated phase change materials, Appl. Therm. Eng. 50 (2013) 555–561.
[15] ANSYS FLUENT Theory Guide Release 13.0, 2010.
[16] T. Bauer, D. Laing, R. Tamme, Characterization of sodium nitrate as phase change material, Int. J. Thermophys. 33 (2012) 91–104.
[17] G.J. Janz, C.B. Allen, N.P. Bansal, R.M. Murphy, R.P.T. Tomkins, Physical properties data compilations relevant to energy storage. 2: Molten salts: data on single and multi-component salt systems, NASA STI/Recon Tech. Rep. N 80 (1979) 10643.
[18] Y. Zheng, W. Zhao, J.C. Sabol, K. Tuzla, S. Neti, A. Oztekin, Encapsulated phase change materials for energy storage – characterization by calorimetry, Sol. Energy 87 (2013) 117–126.
[19] F.P. Incropera, D.P. DeWitt, Fundamentals of Heat and Mass Transfer, fifth ed., John Wiley & Sons Inc., New York, 2002.
[20] A Dowtherm Heat Transfer Fluids by SOLUTIA, Therminol VP-1 (Ed.).
[21] E. Assis, G. Ziskind, R. Letan, Numerical and experimental study of solidification in a spherical shell, J. Heat Transfer 131 (2008) 024502.
[22] M. Ashjaee, S. Amiri, K. Habibi, Slot jet impingement heat transfer from an isothermal circular cylinder, in: Second International Conference on Thermal Issues in Emerging Technologies, 2008, ThETA'08, 2008, pp. 399–404.
[23] E. Buyuk, Heat transfer and flow structures around circular cylinders in cross flow, J. Eng. Environ. Sci. 23 (1999) 299–315.